AIAA JOURNAL
Vol. 42, No. 3, March 2004

Measurements of a Heated Square Jet

L. P. Chua,* Y. F. Li,† and T. Zhou‡
Nanyang Technological University, Singapore 639798, Republic of Singapore

The velocity and temperature measurements of a heated jet issuing from a square nozzle into stagnant ambient air are presented. Measurements were accomplished by means of single hot-wire, single cold-wire, x-wire and three-wire (a cold wire in front of an x wire) probes. The result showed that the jet initial boundary layer was laminar. Mean velocity and temperature reached the self-preservation immediately after the jet potential core. Based on the decay of the local maximum velocity and temperature, as well as the spreading of velocity and temperature half-width, the interaction region was determined to be 8*De*. It was found that the Reynolds normal stress, Reynolds shear stress, and heat flux achieved a self-preservation state at $x = 20De$, $30De$, and $35De$, respectively. The turbulent Prandtl number, which was determined based on the Reynolds shear stress and heat flux, kept approximately constant from the jet centerline until the half-width of the jet and increased thereafter in the outer jet. This finding suggested that some inaccuracies might have incurred in the computation fluid mechanics results by assuming a constant turbulent Prandtl number in the similarity solution of the jet. Last, comparison of velocity half-width along the *y* and *w* axes, as well as the measurements of mean velocity contours at various streamwise locations, indicated that there was an axis switching in the present square jet, although more experimental evidence would be required.

Nomenclature

A_1	=	decay rate of the square jet centerline velocity (or temperature)
A_2	=	spread rate of the square jet velocity (or temperature) half-width
B_1	=	kinematic virtual origin of the square jet
B_2	=	geometric virtual origin of the square jet
De	=	equivalent diameter of a square jet, $(2d/\sqrt{\pi})$, mm
d	=	length of the square jet or the diameter of the circular jet, mm
L_y, L_w	=	velocity half-width, that is, the position where U_0 is reduced to half, along the y and w axes, respectively, mm
Pr_T	=	turbulent Prandtl number
Re	=	Reynolds number, $(U_j De/\nu)$
T	=	instantaneous jet temperature, K
T_j	=	jet exit temperature, K
T_m	=	local mean temperature, K
T_0	=	axial centerline local mean temperature, K
U_j	=	jet exit velocity, m/s
U_m	=	axial mean velocity, m/s
U_0	=	axial centerline local mean velocity, m/s
u	=	instantaneous axial velocity, m/s
u'	=	root mean square of axial velocity fluctuation, m/s
u'_c	=	root mean square of axial velocity fluctuation at centerline, m/s
$u'_{y,\max}$, $u'_{w,\max}$	=	maximum root mean square velocity in the mixing layers at the y and w axes respectively, m/s
$\overline{uv}$	=	Reynolds shear stress, m^2/s^2
v	=	instantaneous lateral velocity, m/s
v'	=	root mean square of lateral velocity fluctuation, m/s
v'_c	=	root mean square of lateral velocity fluctuation at centerline, m/s
w	=	axis parallel to the diagonal of the square nozzle, mm
x, y, z	=	Cartesian coordinate system defined in Fig. 1, mm
y'', w''	=	y and w axes with origins start from the nozzle lip, mm
α	=	temperature coefficient of resistivity, K^{-1}
α_T	=	eddy diffusivity for heat, m^2/s
δ_{my}, δ_{mw}	=	boundary-layer momentum thickness at y and w axes respectively, mm
θ	=	root mean square of temperature fluctuation, K
θ_c	=	root mean square of centerline temperature fluctuation, K
ν	=	kinematic viscosity, m^2/s
ν_T	=	eddy diffusivity for momentum, m^2/s
$\overline{v\theta}$	=	heat flux, mK/s

Received 31 July 2001; revision received 1 February 2003; accepted for publication 4 April 2003.

*Associate Professor, School of Mechanical and Production Engineering, Nanyang Avenue; mlpchua@ntu.edu.sg.

†Ph.D. Student, School of Mechanical and Production Engineering, Nanyang Avenue.

‡Assistant Professor, School of Mechanical and Production Engineering, Nanyang Avenue.

Introduction

NONCIRCULAR jets have been identified as an efficient technique of passive flow control that allowed significant improvements of performance such as reducing combustion instabilities and undesired emissions, noise suppression, and thrust vector control, at a relatively low cost, which rely solely on changes in the geometry of the nozzle. It is then not unexpected that noncircular jets had been the topic of extensive research in the past 15 years.[1] However, among noncircular jets, there has been relatively less experimental measurements on square jet apart from the studies of Tsuchiya et al.,[2] Quinn and Militzer,[3] Gutmark et al.,[4] Quinn,[5] and Grinstein et al.[6] The measurements of Tsuchiya et al.[2] and Gutmark et al.,[4] however, were mainly on rectangular and triangular jets, respectively, with square jets being just a small part. There has also been a lack of temperature measurements, especially heat flux distributions, in the literature. Most of the measurements are on the velocity alone, except Tsuchiya et al.,[2] who has done some temperature measurements on the rectangular jet, but again not the square jet. Note that nearly all of the measurements have been done on the square orifice plate rather than a contour square nozzle. Furthermore, the measurements of these studies were focused on the mixing layers

and, relatively, at the near field. The main objective of this paper, thus, is to present the measurements of the mean velocity, mean temperature, Reynolds normal and shear stresses, heat fluxes, and, hence, a subsequent determination of turbulent Prandtl number at the far field of the contour square jet. The turbulent Prandtl number, which was an important parameter in computational fluid mechanics, was usually assumed a constant value in the calculation. There was, however, a lack of measurements of this prime parameter in the literature. The self-preservation of the decay rate of the centerline mean velocity and mean temperature, as well as the spreading rate of the velocity and temperature half-width, are also presented.

One of the most intriguing aspects of noncircular jet is the phenomenon of axis switching, which is of interest from a fundamental scientific viewpoint and for its applications in enhancing entrainment, mixing, and turbulence production. The second objective of the paper is to present a preliminary study on the axis-switching phenomenon of the contour nozzle square jet as compared to an orifice square jet. For this purpose, mean velocity profiles across the diagonal (defined as the w axis) of the jet were measured, and the corresponding half-width was determined and compared with L_y. This was because the axis switching would cause a 45-deg rotation of the axes,[7] resulting with the orientation of the mean velocity profiles resembling the original square nozzle shape (shown subsequently) at $x = 0.5De$ and rotating 45 deg to form a rhombus shape (with 90 deg at the four corners), at $x = 4De$. Through the measurements of the half-width along the y and w axes, the streamwise distributions of L_y and L_w would cross each other if the axis switching occurred. The effect of the jet initial condition, such as the turbulence intensity at the jet exit, and the ratios of De/δ_{my} and δ_{mw}/δ_{my} on the axis switching has been investigated in detail and compared with those of Grinstein et al.[6] It was found that, although the high δ_{mw}/δ_{my} ratio has the adverse effect to initiate early axis switching, the high De/δ_{my} ratio and low turbulence intensity of the present jet caused the first axis switching at about $1.75De$ and subsequently at $5De$. The mean velocity contours at a few streamwise locations are also presented to search for the evidence of the axis switching. However, the mean velocity contour, as well as the half-width, which is based on the mean velocity profiles, was found not to be a sensitive indicator of axis switching. More careful and extensive measurements on the velocity spectrum and streamwise vorticity were required for a conclusive finding on the axis switching and its mechanism.

Experimental Method

Measurements were taken on the air jet supplied by a centrifugal blower through a 25-mm square nozzle (of equivalent diameter $De = 28.2$ mm) fabricated from fiberglass with an area contraction ratio of 100:1. The contour was designed according to the incompressible axisymmetric potential flow theory[8] to 1) avoid flow separation in the construction and 2) achieve uniform flow at the exit. Installed between the blower and nozzle were a divergence section, settling chamber of size $250 \times 250 \times 250$ mm^3, screens, and honeycomb section to convey the flow and reduce turbulence. A variable speed alternating current three-phase induction motor was selected to drive the blower, and motor speed regulation was achieved through a frequency control system using pulse width modulation inverter. The jet exit velocity U_j was set at 31 ± 0.5 m/s, and the corresponding Reynolds number was 5.75×10^4. The air was heated with a 1-kW electrical coil element situated at the inlet of the blower to ensure a better mixing of the heated air before the entry into the settling chamber. The temperature of the heated air could be controlled by means of thermostat through a thermocouple installed in the air duct. Furthermore, the entire jet assembly was wrapped

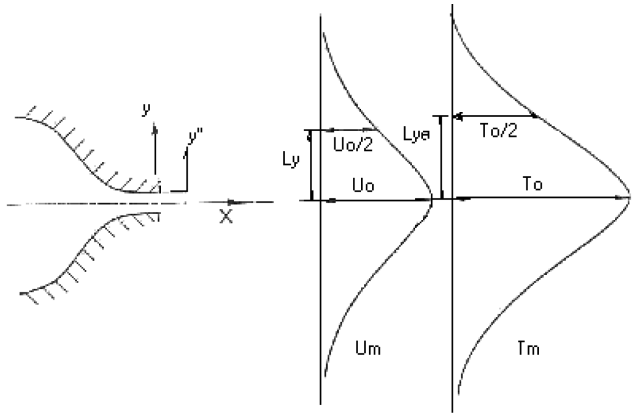

Fig. 1a Square jet coordinate, as well as the jet velocity and temperature profiles.

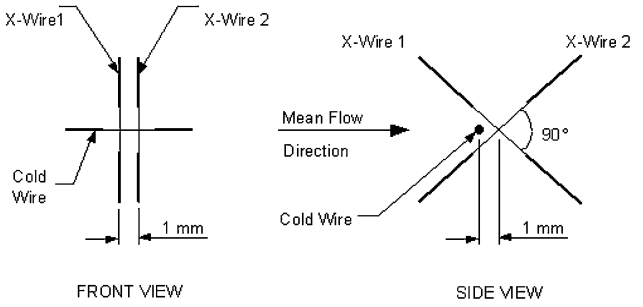

Fig. 1b Three-wire probe.

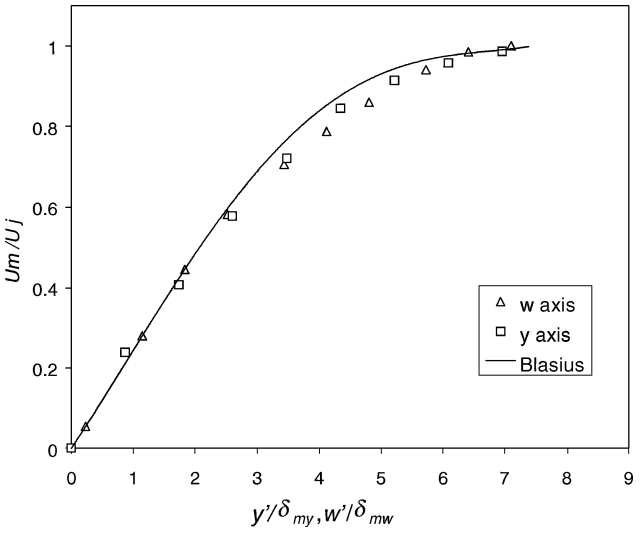

Fig. 2 Comparison of velocity profiles in y and w axes at the nozzle exit with Blasius solution.

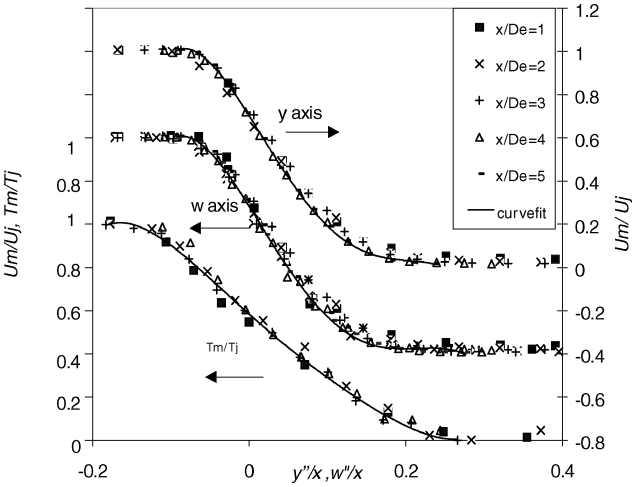

Fig. 3 Distributions of mean velocity (in y and w axes) and temperature in jet mixing layer.

with three layers of fiberglass, which was enough to eliminate the buoyancy effect, and further increment in the number of insulation layers was found to have no significant improvement in preventing heat loss from the test rig assembly.[9] The temperature at the nozzle exit was set at $20 \pm 0.5^{\circ}$C above the ambient air, and it took about an hour to have a uniform temperature distribution along both the horizontal and vertical axes at the jet exit. The jet nozzle, velocity, and temperature profiles are shown in Fig. 1a.

Instantaneous velocities of the jet were acquired through single hot-wire probe (ϕ5-μm Wollaston Pt 10%–Rh, with length about 1.0 mm) connected to a constant temperature anemometer (CTA) module operating at an overheat ratio of 1.5. For the x-wire probe, the included angle of the two wires was about 90 deg, and the separation between the two wires was about 1.0 mm. For the three-wire measurements, the cold wire (ϕ1.2-μm Wollaston Pt 10%–Rh, with length about 1.5 mm) was located about 1 mm in front of the center of the x wire as shown in Fig. 1b. The probe (for the four different types of wire, single hot wire, single cold wire, x wire and three wire) was mounted onto a dial height gauge fixed to a traversing mechanism capable of traveling in three perpendicular directions, x, y, and z axes. An attachment on the height gauge enabled data in the w axis (which was the axis parallel to both the square nozzle diagonal and the y–z plane, i.e., inclined at 45 deg to the z axis) to be captured for the axis-switching investigation.

The hot wire was calibrated before each measurement set in the potential core with reference to a pitot–static tube connected to a pressure transducer. For single hot-wire measurements, voltages from the CTA and pressure transducer were digitized by a 12-bit analog-to-digital converter before input into a computer for processing. After calibration constants were computed using the least-squares method, they were then fed into the second part of the computer program, which converted hot-wire voltages into velocities. For the x-wire and three-wire measurements, in addition to obtaining the usual calibration constants, the x-wire probe was calibrated for velocity and yaw in the potential core of the jet, with the range of yaw angles −15–15 deg in 3-deg steps. Voltages from the single-wire, x-wire, and three-wire probes were passed through low-pass filters before digitizing into a computer using a National Instrument model. The sampling frequency was double the cutoff frequency (1600 Hz), and the recording time was 5 s for single wire, 10 s for the x wire, and 15 s for the three wire. Digitized hot-wire and cold-wire voltages were converted to velocity and temperature, respectively. The statistical parameters such as mean, root mean square, and cross correlation of the u and v, as well as v and T, were obtained using a MATLAB® program.

Results and Discussion

The mean axial velocity across the immediate exit of the square nozzle had a top-hat shape and is symmetrical about the jet centerline. On the centerline of the nozzle exit, the turbulent intensity u'/U_j (single prime denoting rms values) was measured to be

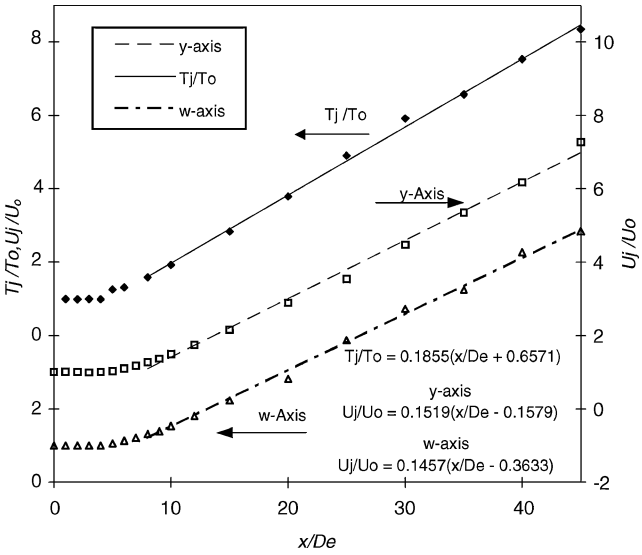

Fig. 5 Variation of jet centerline mean velocity (in *y* and *w* axes) and temperature along the streamwise direction.

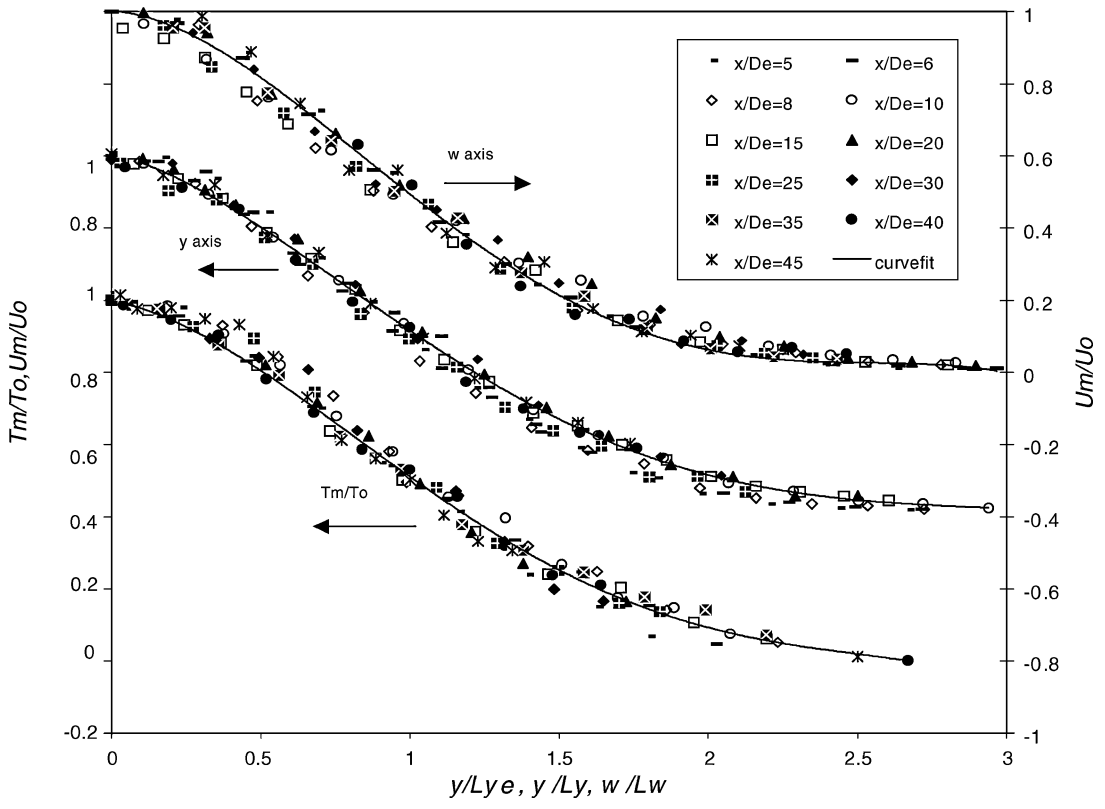

Fig. 4 Distributions of mean velocity and temperature from 5*De* to 45*De*.

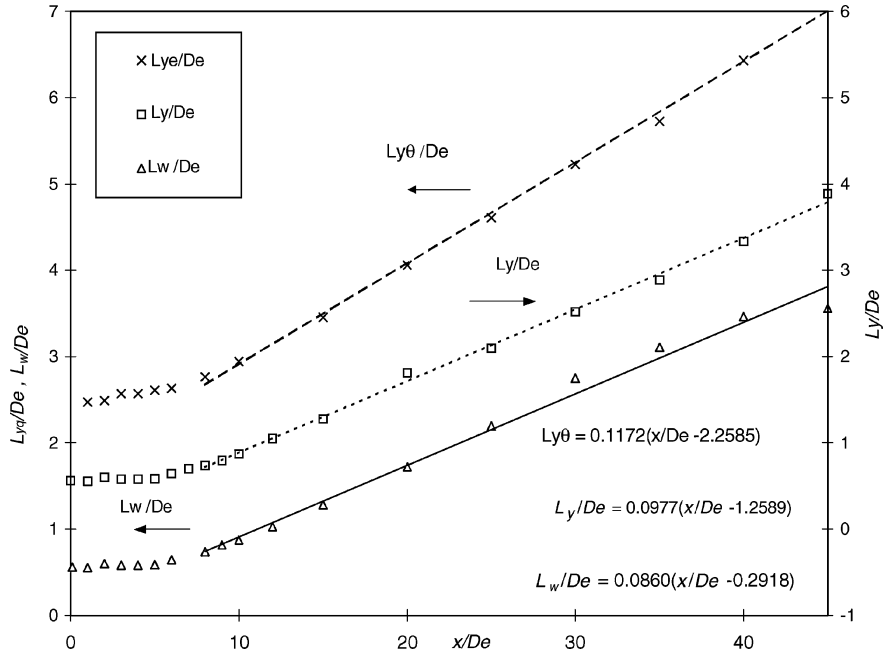

Fig. 6 Variation of jet velocity (in y and w axes) and temperature half-width along the streamwise direction.

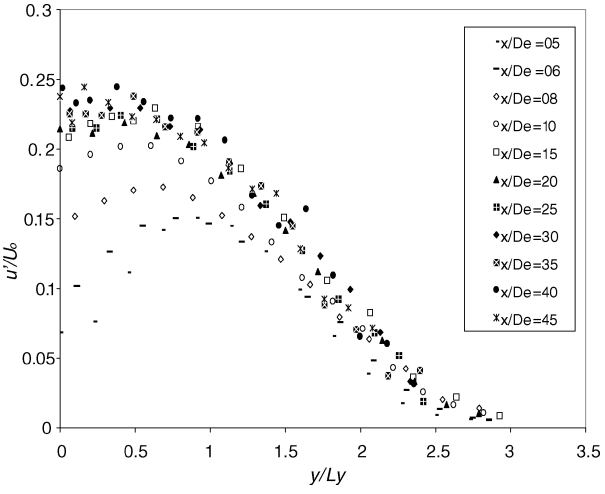

Fig. 7 Distributions of u'/U_0 along y axis at various streamwise locations.

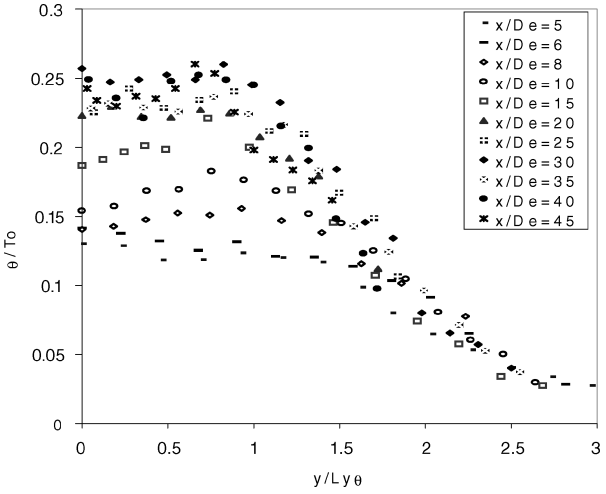

Fig. 9 Distributions of rms temperature along y axis at various streamwise locations.

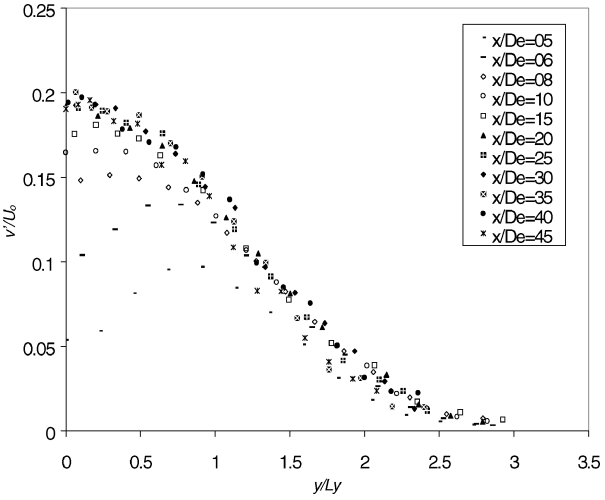

Fig. 8 Distributions of v'/U_0 along y axis at various streamwise locations.

approximately 1.0%. Estimates of the random component of uncertainty for mean and rms velocities (temperature) were ±1.1 (±1.6) and ±3.9% (±2.0%), respectively. When the method of propagation of errors was used, the experimental uncertainty in u'/U_0, v'/U_0, and θ/T_0 were estimated to be ±4.1, ±4.5, and ±2.5%, respectively, from uncertainties in the mean and rms velocities.[10] With use of the same method, the experimental uncertainty for the decay rate, spreading rate, $\overline{uv}/U_0^2$, $\overline{v\theta}/U_0T_0$, and turbulent Prandtl number were correspondingly estimated as ±4.9, ±5.1, ±6.5, ±5.4, and ±7.1%. Figure 2 shows good agreement of the jet boundary layer with Blasius' solution for a flat plate. The normalizing scale was the boundary-layer momentum thickness, which was evaluated to be 0.115 (δ_{my}) and 0.413 mm (δ_{mw}) for the y and w axes, respectively.

Mean velocity and temperature profiles of the quasi-two-dimensional mixing layer near the nozzle exit are presented in Fig. 3. Note that y'' and w'' were measured outward from the nozzle wall (Fig. 1a). Although the dimensionless quantities y''/x and w''/x relate to the mixing layer, their use in the interaction region can indicate the degree of departure from the self-preserving mixing layer. Observe that the mean velocity (temperature) profiles in the mixing layer became self-similar at $4De$ and $3De$ ($3De$) for the y and w axes, respectively. Also observe that the temperature profiles

are much steeper than those of the velocity, indicating that the heat transfer is more efficient than the momentum in the mixing layer.

The mean velocity and temperature profiles in the range $5 \leq x/De \leq 45$ are shown in Fig. 4. Here, the local centerline mean velocity U_0, local centerline mean temperature T_0, velocity half-width L_y (or L_w), and temperature half-width $L_{y\theta}$ are the normalizing coordinates. As evident in Fig. 4, the mean velocity and temperature distributions collapse onto a single curve, indicating that U_m and T_m reach self-preservation at the end of potential core, that is, $x = 5De$. There also is slightly more scatter in the w axis distribution than in the y axis for velocity.

With the framework of self-preservation, the equations for the conservation of momentum and heat are satisfied, on a local and integral basis, if U_0, $T_0 \sim x^{-1}$ and L_y, L_w, $L_{y\theta} \sim x$. Figure 5 shows the variation of centerline mean velocity U_0 (and centerline mean temperature T_0) in the y and w (and y) directions vs x/De. The centerline mean velocity U_0 in the range $8 \leq x/De \leq 45$ collapses reasonably well onto a straight line, which can be expressed as

$$U_j/U_0 = A_1[(x/De) + B_1] \tag{1}$$

where A_1 and B_1 are the decay rate and the kinematic virtual origin of the jet, respectively. In the experiment, decay rates for U_0 should be the same for both axes, the slight discrepancy (of 4%) could be attributed to experimental uncertainty. In addition, self-preservation of U_0 at $x \approx 8De$ indicates that the interaction region of the present square jet is rather short. The decay of the centerline mean temperature T_0, which can be expressed as

$$T_j/T_0 = A_1[(x/De) + B_1] \tag{2}$$

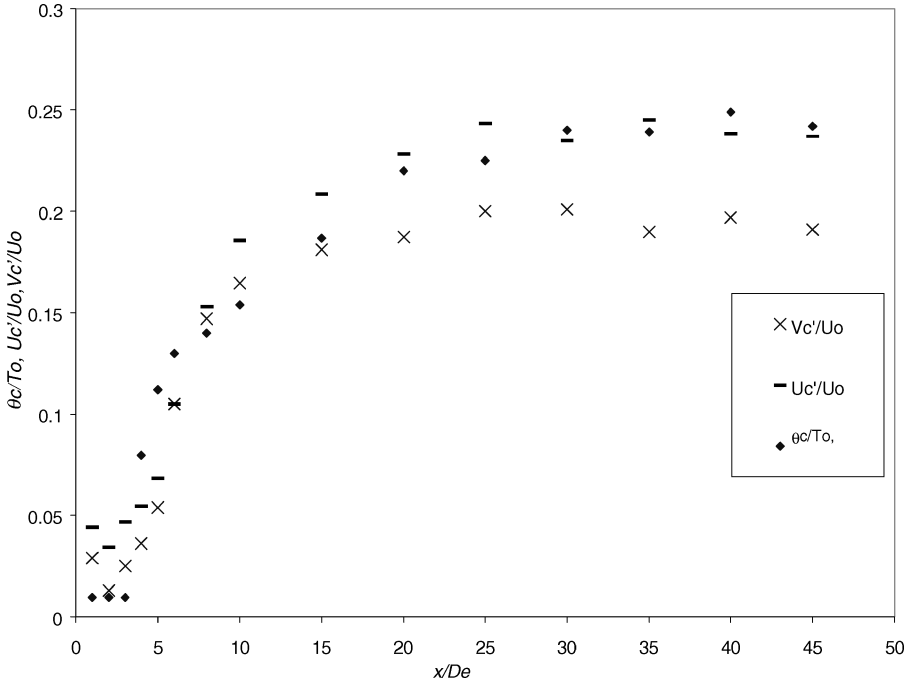

Fig. 10 Streamwise distributions of centerline rms temperature and axial and lateral rms velocity.

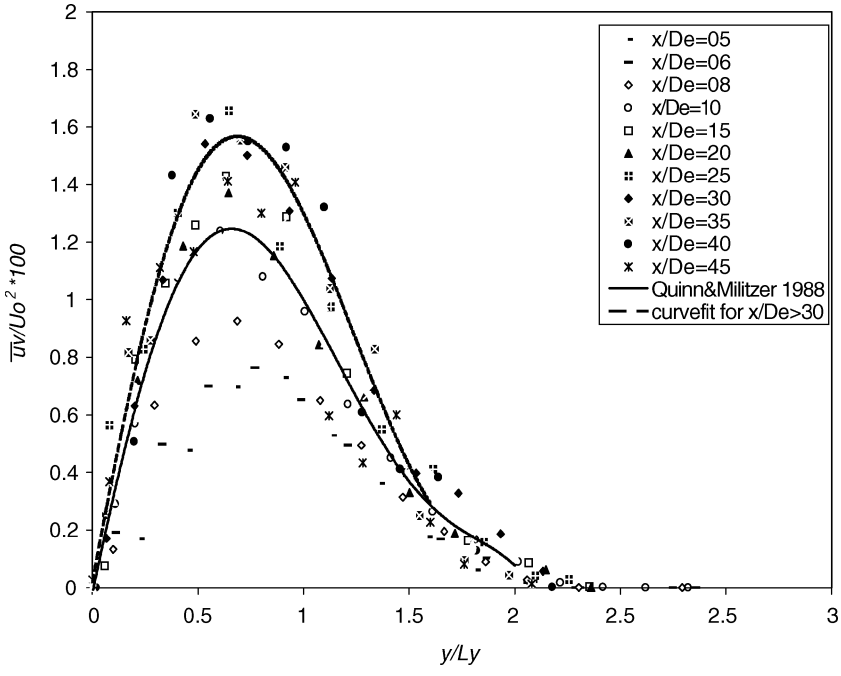

Fig. 11 Streamwise distribution of normalized Reynolds shear stress $\overline{uv}$ along y axis.

collapses reasonably well into a straight line within the same range of $8 \leq x/De \leq 45$ as the centerline mean velocity. The gradient of the centerline mean temperature decay is, however, greater than those of the velocity counterpart. This indicates that the heat transfer is more efficient than the momentum transfer.

Figure 6 shows the evolution of the half-width variation in the streamwise direction. The linear relationship is now given by

$$L/De = A_2[(x/De) + B_2] \tag{3}$$

where A_2 and B_2 in the equation are the jet spreading rate and geometric origin. Figure 6 shows that self-preservation has been achieved at streamwise location of $x/De = 8$. Again, the spreading rate of the temperature half-width is much faster than that of the velocity, as can be observed in Fig. 6.

In Table 1, the current results are presented along with results of other investigators (Refs. 2, 3, 11, and 12). When the entries are compared, differences between the decay and spreading rates for the current square jet and those of other researchers are seen to be relatively small. The centerline mean velocity has a slightly

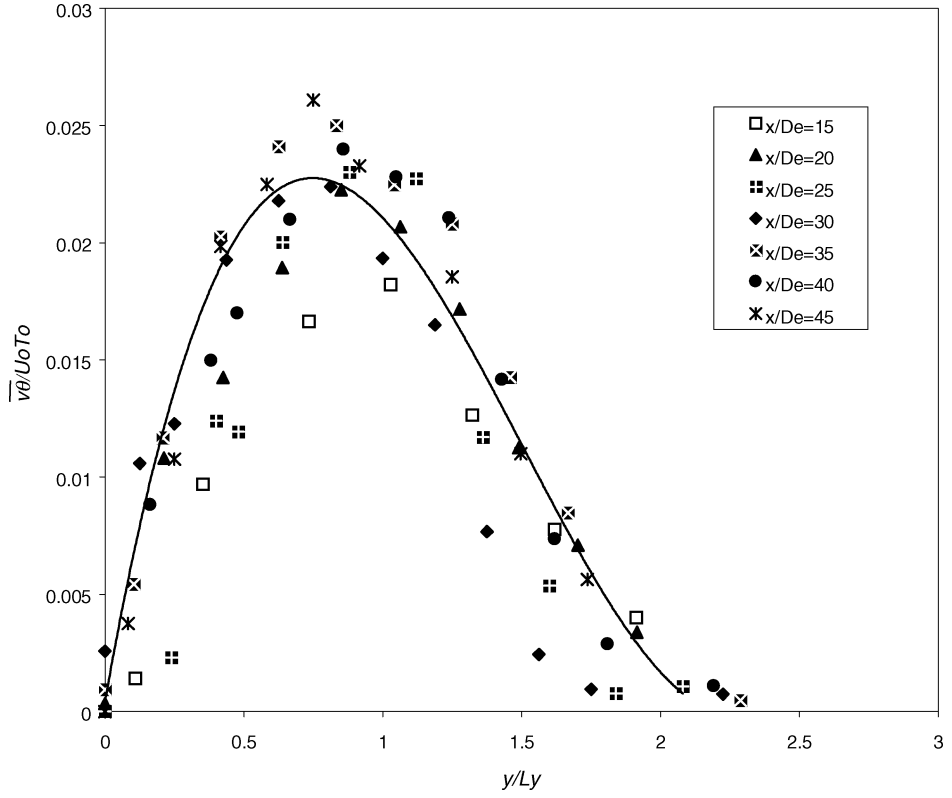

Fig. 12 Streamwise distribution of normalized heat flux $\overline{v\theta}$ along y axis.

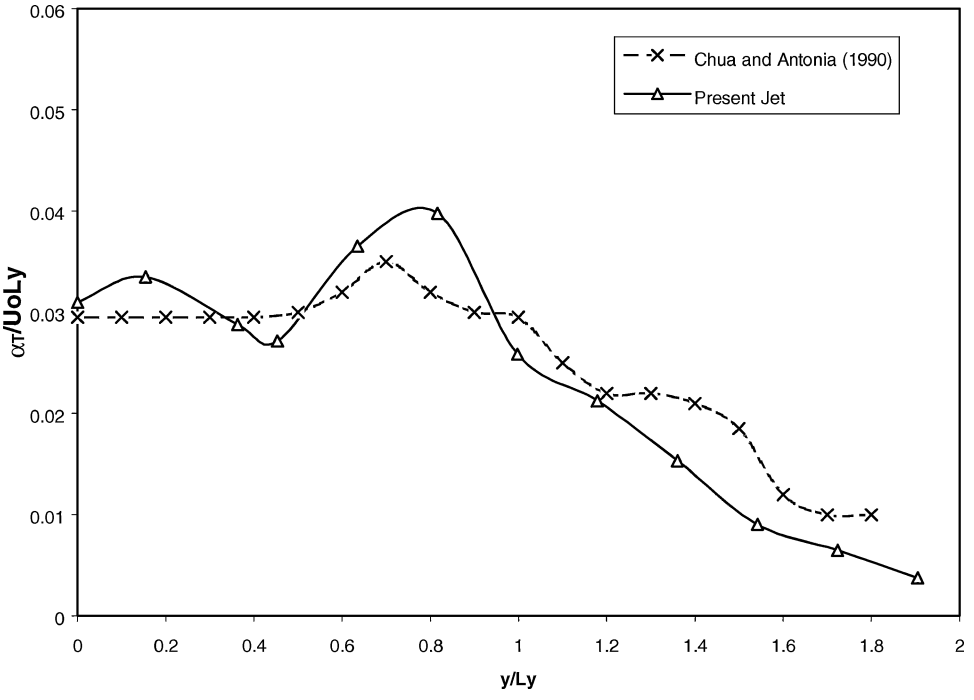

Fig. 13 Variations of turbulent momentum diffusivity along y axis.

Table 1 Comparison of present results with those of other researchers

Investigator	Initial condition	Reynolds number	A_1	B_1	A_2	B_2	Range
Yevdjevich[11]	Turbulent	——	0.1430	0.000	——	——	$20 \le x/De \le 200$
Du Plessis et al.[12]	Orifice type	2.82×10^4	0.1386	−0.0844	0.085	−1.3775	$8 \le x/De \le 22$
Tsuchiya et al.[2]	Orifice type	1.55×10^4	——	——	0.0826	0.4116	$6 \le x/De \le 30$
Quinn and Militzer[3]	Sharp edge	1.84×10^5	0.1850	−0.150	——	——	$8.4 \le x/De \le 62$
	slot	1.84×10^5	——	——	0.0870	0.650	$9.8 \le x/De \le 22.4$
Present work							
Velocity y axis	Laminar	5.75×10^4	0.1519	−0.1579	0.0977	−1.2589	$8 \le x/De \le 45$
Velocity w axis	Laminar	5.75×10^4	0.1457	−0.3633	0.0860	−0.2918	$8 \le x/De \le 45$
Temperature	——	——	0.1855	0.6571	0.1172	−2.2585	$8 \le x/De \le 45$

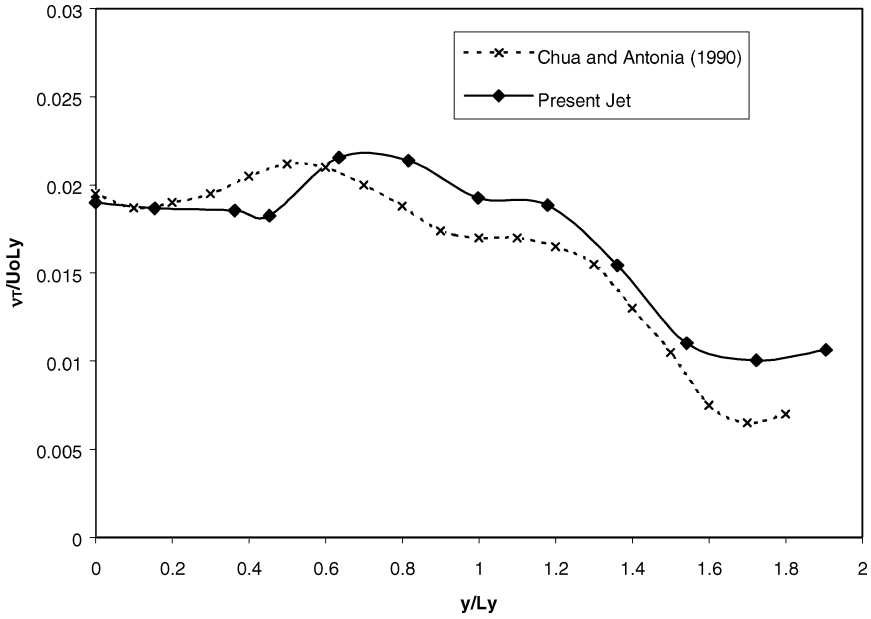

Fig. 14 Variations of turbulent heat diffusivity along y axis.

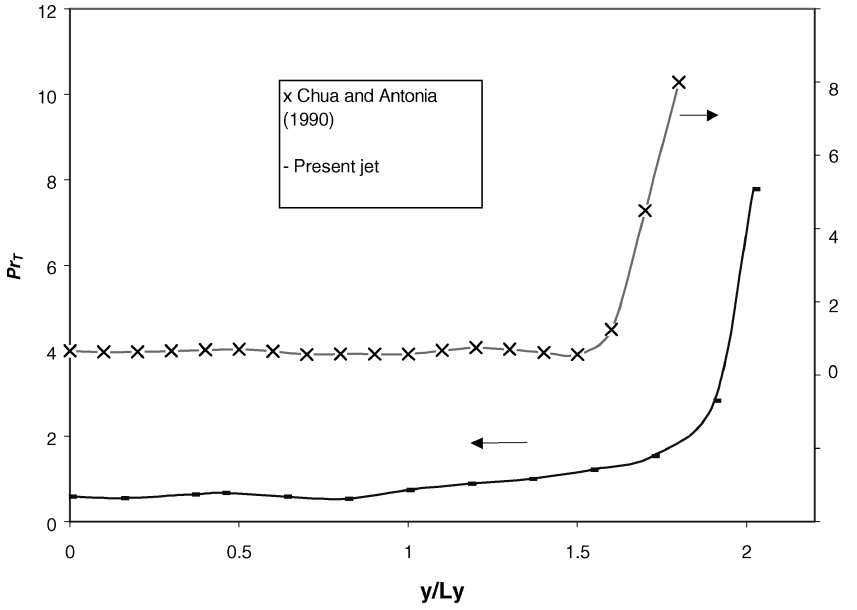

Fig. 15 Variations of turbulent Prandtl number along y axis.

higher decaying rate as compared with DuPlessis et al.[12] with about half of the present Reynolds number. The present decaying rate is, however, lower than that of Quinn and Militzer[3] with three times higher Reynolds number. Regardless of the other jet initial conditions, it seems that the higher the Reynolds numbers, the higher the decaying rate is of the local maximum mean velocity. The present square jet has a slightly higher spreading rate than those of the other researchers. These may be due to the difference in the jet initial condition, such as its boundary-layer thickness and turbulence level.[13] Note that for most of the other investigators listed in Table 1, the square jet is mainly the slot jet with very thin or no boundary layer. Also note that the gradients of the centerline mean temperature decay and the temperature half-width spreading rate are, in general, higher than those of the velocity counterpart found in the literature. There is lack of temperature measurements of the square jet reported in the literature, thus, making comparison with other researchers difficult.

Figures 7 and 8 show the distributions of u'/U_0 and v'/U_0, respectively. Observe that both distributions increased from $5De$ and reach self-preservation at $25De$ and $20De$, respectively, for u'/U_0 and v'/U_0. The shape of the v'/U_0 distributions changes from saddlelike with the peak at about $y/L_y = 1$ at $5De$ to a Gaussian shape with the peak slowly shifting toward the centerline. Unlike v'/U_0, which monotonically decreases from the centerline once it reaches the self-preservation state, the distributions of u'/U_0 show a small peak at about $0.5L_y$. The distributions of u'/U_0 reach a peak of about 0.24, which is higher than the peak of about 0.2 for v'/U_0. These results indicate that the fluctuations of the axial velocity have higher kinetic energy than the lateral velocity. The distributions of θ/T_0 are shown in Fig. 9. When the root mean square velocity distributions are compared, the profiles of θ/T_0 at small streamwise locations are relatively flat without any obvious peak until $8De$. The root mean square temperature distributions reach self-preservation at about $20De$, and the profiles exhibit a vague peak at about $y/L_\theta = 1$; this is, again, different from the v'/U_0 with a monotonous decrease from the jet centerline.

Figure 10 shows the streamwise distributions of the centerline axial and lateral root mean square velocities and temperature. Both of centerline root mean square axial velocity and temperature distributions reach an asymptotic value of 0.24 at $25De$, whereas the lateral root mean square velocity has constant values of about 0.19 at similar streamwise locations.

Figure 11 shows the distributions of normalized Reynolds shear stress $\overline{uv}$ at various x/De locations. Note that the absolute values of $\overline{uv}$ presented in Fig. 11 are symmetrical about the centerline. Also the distributions obtained by Quinn and Militzer[3] at about $13De$ and a best-fit curve for the Reynolds shear stresses higher than $30De$ are shown in Fig. 11. The Reynolds shear stress has increased from $5De$ and reached self-preservation at about $30De$. The location of the Reynolds shear stress peak has also shifted from about $1.0L_y$ to $0.8L_y$. The peak of the Quinn and Militzer distribution has only reached 0.012 at about $0.7L_y$; this is not totally unexpected because the measurements have been done at about $13De$ and should not have reached the self-preservation state at this low streamwise location. The heat flux distribution, which is normalized by both the local centerline mean velocity U_0 and temperature T_0, is shown in Fig. 12. Observe that the normalized heat flux distribution has reached self-preservation at about $35De$ in Fig. 12. Both the Reynolds shear stress and heat flux distributions show some scatter, especially at the high streamwise location, for example, $45De$. This is due to the fast decay of the mean velocity, $U_0 = 3.5$ m/s, and temperature, $T_0 = 1.8$ K at these locations. Furthermore, the jet is a high turbulence intensity flow, for instance, at $40De$, the u'/U_m (v'/U_m) and θ/T_m is about 0.24 (0.20) at the jet axis, as shown earlier in Fig. 10. At the jet half-width, the values of u'/U_m, v'/U_m, and θ/T_m increase to 0.50, 0.34, and 0.39, respectively. Such high fluctuations coupled with the fact that flow reversal starts to occur at the half-width location, as found by Chua and Antonia,[14] all have contributed to the difficulty in measurements. Because the velocity vector angle at these locations may be over 90 deg, the included angle of the 120-deg x wire may be more suitable for the present measurements.[15]

With the measured Reynolds shear stress and the heat flux, the eddy diffusivity for momentum and heat can be obtained as

$$\nu_T = -\frac{\overline{uv}}{(\partial U_m/\partial y)} \tag{4}$$

$$\alpha_T = -\frac{\overline{v\theta}}{(\partial T_m/\partial y)} \tag{5}$$

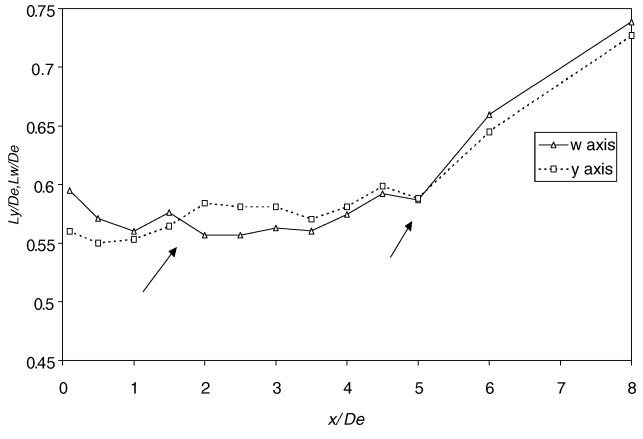

a)

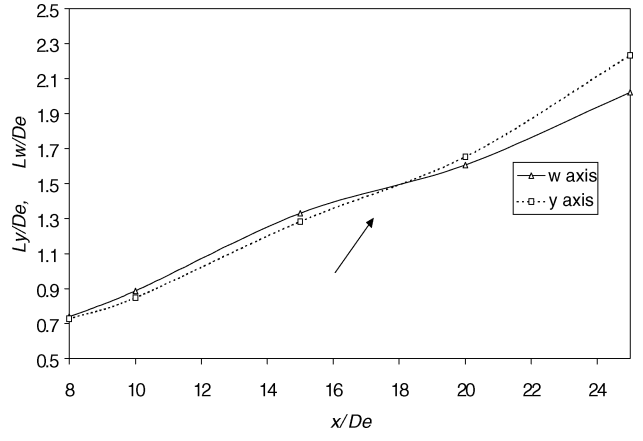

b)

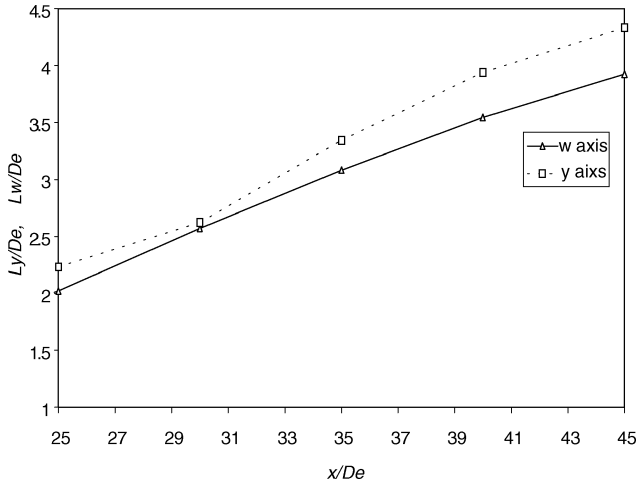

c)

Fig. 16 Comparison of half-widths in *y* and *w* directions for a) $0.1 \le x/De \le 8$, b) $8 \le x/De \le 25$, and c) $25 \le x/De \le 45$.

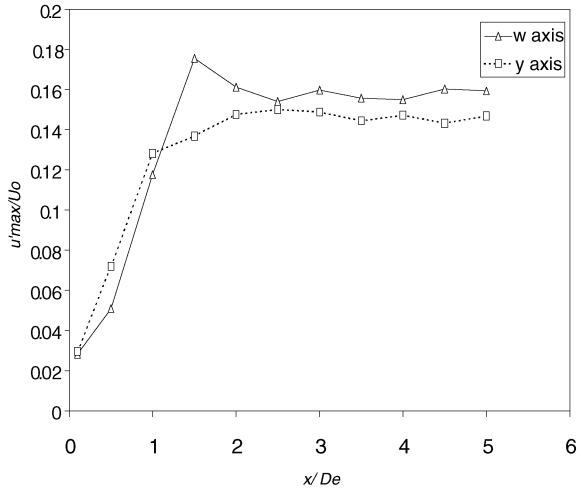

Fig. 17 Comparison of maximum turbulent intensities in the shear layer along *y* and *w* axes.

Consequently, turbulent Prandtl number Pr_T, defined as the ratio of eddy diffusivities for momentum and heat, can be written as

$$Pr_T = \nu_T/\alpha_T \tag{6}$$

Note that both $\partial U_m/\partial y$ and $\partial T_m/\partial y$ (also $\overline{uv}$ and $\overline{v\theta}$) are obtained from Fig. 4 (Figs. 11 and 12) with the fourth-order polynomial fitted to the U_m/U_0 and the T_m/T_0 distributions for $35 \le x/De \le 40$. In both cases, the limiting values of these quantities at $y/L_y = 0$ are obtained using the L'Hopital rule. Note that the range of x/De selected is based on the attainment of self-preservation of Reynolds shear stress and heat flux at these streamwise locations. The distributions of turbulent momentum and heat diffusivities are shown in Figs. 13 and 14, respectively. The results of circular jet from Chua and Antonia[16] are also shown. Observe that both the turbulent momentum and heat diffusivities of the circular and square jets have a similar trend. However, the peaks of the present jet are slightly shifted to the left due to both the maximum Reynolds shear stress and heat flux happening at higher y/L_y locations. Note that the results of Chua and Antonia were obtained at the self-preservation region of the circular jet, which is achieved at a much earlier streamwise station at $x/d = 15$ as compared to the present jet. The distributions of turbulent Prandtl number Pr_T are shown in Fig. 15. For comparison, the distribution of Prandtl number of the circular jet[16] is also shown. Figure 15 shows that Prandtl number is not constant across the y axis of the jet. Rather, the quantity maintains at about a constant value of 0.6 before rising gradually after $y/L_y = 1.0$. This implies that the turbulent Prandtl number Pr_T, which is an important parameter for similarity solutions of nonisothermal square jets, should not be taken as a constant. Within the region $y/L_y = 1.0$, or at most extending to about $y/L_y = 1.4$, the error in obtaining the mean temperature and heat flux profiles using computation fluid mechanics of the square jet may be negligible. However, significant deviation from the actual flow may arise if Pr_T is taken as the same constant value beyond the range in the simulation.

To study axis-switching characteristics of a square jet, the variations of L_y/De and L_w/De against x/De are compared in a graph, and the intersections of the two curves indicate the locations of axis switching. Figures 16a–16c show the distributions of L_y/De and L_w/De along the streamwise directions. Observe in Fig. 16a that L_w decreases from the jet exit to $1De$ and then follows with a gentle increase until $5De$ with an obvious hump at $1.5De$. On the contrary, L_y decreases slightly from the jet exit, followed by increasing from $0.5De$ to $2De$, and then maintains at about the same level till $3De$. A slight dip can be found at $3.5De$ before increasing more steeply to $4.5De$. Following a small dip at $5De$, L_y then increases sharply thereafter. The profiles of L_y/De and L_w/De are, thus, the first and second crossovers at about $1.75De$ and $5.0De$, respectively. The third crossover is at $17.5De$, as shown Fig. 16b, and the variations of L_y/De and L_w/De are about parallel to each other without any crossover, as demonstrated in Fig. 16c.

It is obvious from Fig. 16a that the first crossover has happened with the shrinking of L_w and the faster growth rate of L_y. Note, however, that the faster growth of L_y does not happen immediately after the jet exit but at a later streamwise location of $0.5De$. Grinstein et al.[6] have studied the effects of the initial conditions, for example, the turbulence intensity at the jet exit and the ratios of De/δ_{my} and δ_{mw}/δ_{my}, on the axis-switching of the square jet. Table 2 shows a comparison of the initial conditions of the three experimental results of unforced square jets[6] with the present jet. According to the linear stability analysis of Koshigoe et al.,[17] the high δ_{mw}/δ_{my} ratio for the present jet does not favor axis switching. Because the azimuthal nonuniformities of the initial shear layer are quite high, the amplification rates of the corresponding unstable eigenmodes may not be comparable, and the resulting growth rates of the velocity fluctuations associated with the different modes may also not be comparable. However, as can be seen from Table 2, the initial conditions of Reynolds number and u'/U_0 of the present jet are similar to the orifice jet OU1. Furthermore, the value of De/δ_{my}

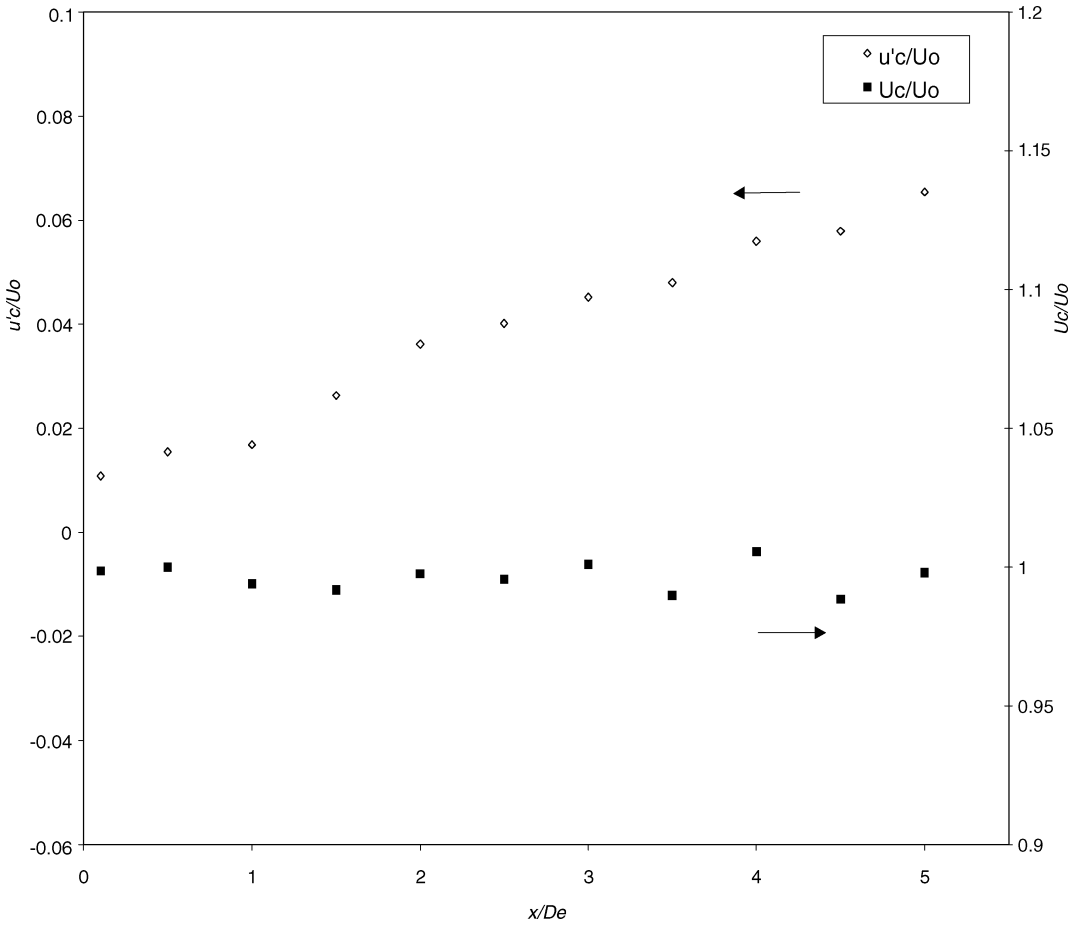

Fig. 18 Centerline variations of mean velocity and normal shear stress in the potential core.

is even much higher than that of OU1. The large De/δ_{my} and low u'/U_0 should have caused the faster growth rate of L_y and resulted in the first axis switching as reported by Grinstein et al. for their OU1 orifice low turbulent square jet.

Figure 17 shows the variations of maximum turbulent intensities of both y and w axes in the mixing layer, which indicate the initial amplification of turbulence along the shear layers. Observe in Fig. 17 that the differences between the amplification rate at the side (y axis) and diagonal (w axis) directions are not obvious. This is different from that of the OU1 (Grinstein et al.[6]). However, the maximum shear stress is consistently higher for the y axis than that of the w axis until $1\,De$, and after that, the shear stress for the w axis is higher than the y axis but maintains about the same level after $2De$. Figure 18 shows the variations of the centerline mean velocity and turbulent intensity. The centerline mean velocity has slight variation around U_j within the potential core as expected. The centerline normal shear

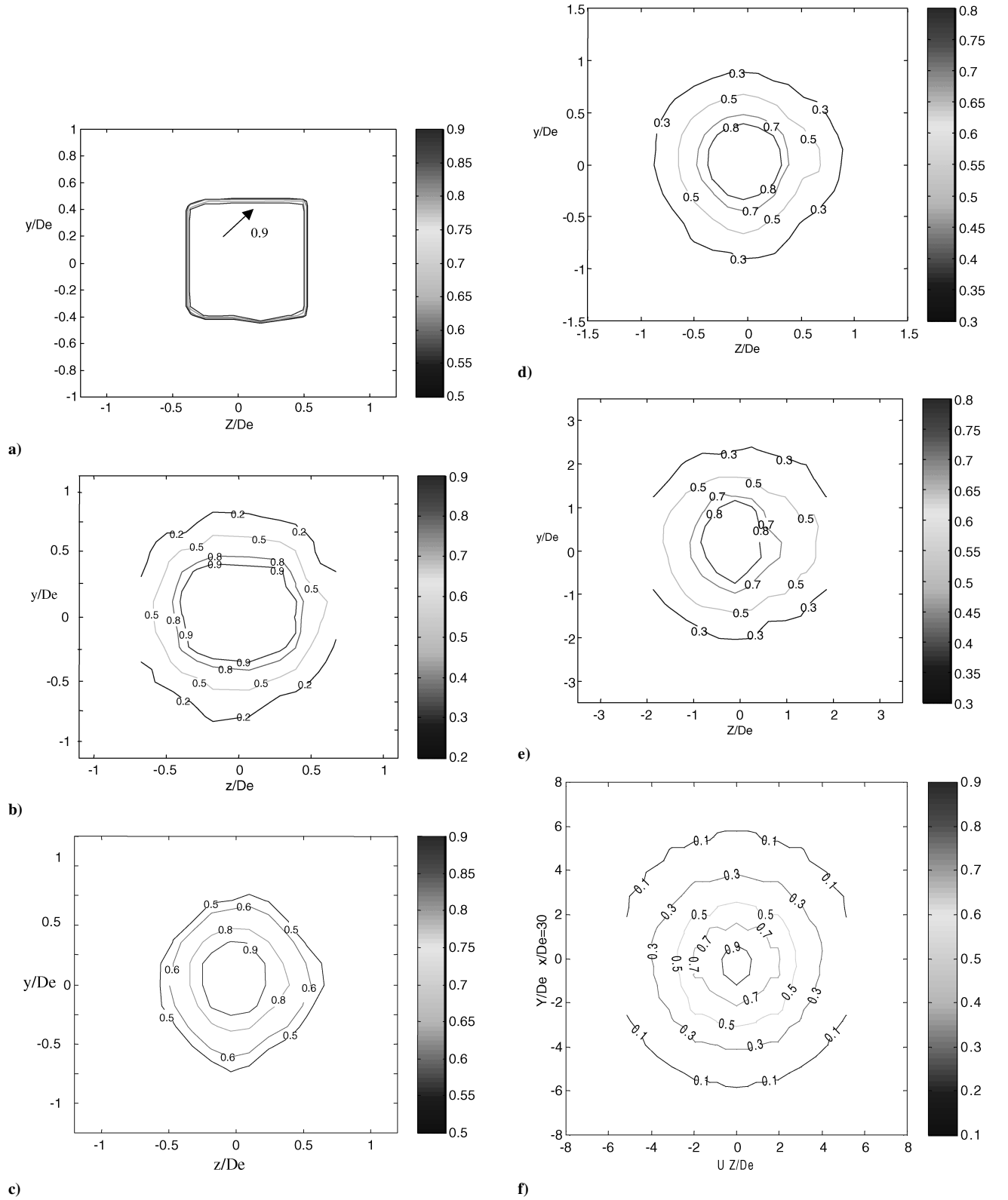

Fig. 19 Contours of normalized mean velocity U_m/U_j (or U_m/U_0) at streamwise locations of a) $0.5De$ (contours varied from 0.9 to 0.3 at 0.2 step from inner to outer contours), b) $2De$, c) $4De$, d) $6De$, e) $20De$, and f) $30De$.

Table 2 Comparison of jet initial conditions with those of Grinstein et al.[6]

Jet	Reynolds number	δ_{mw}/δ_{my}	D_e/δ_{my}	u'/U_0	Crossovers at x locations (in terms of De)
Orifice, OU1	4.2×10^4	1.58	164	0.003	0.3, 14
Slot, OU2	9.3×10^3	1.08	60	0.1	0.6, 3.6, 5.0
Pipe, PU1	9.3×10^3	1.34	40	0.1	None
Contour, present	5.75×10^4	3.5	245	0.01	1.75, 5.0, 17.5

stress has increased continuously along the streamwise direction. The localized changes in the amplification rate are attributed to the axis-switching dynamics and the shear layer amplification.[6] All of these should have overcome the adverse effect of the high δ_{mw}/δ_{my} ratio and contributed positively the axis switching of the present contour nozzle square jet.

To further investigate the axis switching of the present jet, the mean axial velocity profiles at the cross section of $x/De = 0.5$, 2.0, 4.0, 6.0, 20.0, and 30.0 are measured, and the corresponding velocity contours are presented in Figs. 19a–19f. Observe in Fig. 19a that at $x = 0.5De$ the velocity contours maintain the original orientation of the jet. Farther downstream, at $x = 2De$ (Fig. 19b), there is a change in orientation of the velocity contours for U_m/U_j less than 0.5, although the higher level velocity contours (for U_m/U_j greater than 0.8) still maintain the original orientation. It is then obvious in Fig. 19c that there is a clear switching of the axis, with the velocity contours are now resembling a square rotated 45 deg at $4De$. Note that it is not quite possible to have the distributions of the velocity contours with all of the sides straight and resembling a perfect rotated square. The velocity contours of OU1 (Grinstein et al.[6]; see their Fig. 10), although appearing perfect, have been obtained with the assumptions of symmetry and joining the locations of the selected level of contours with straight lines. For the velocity contour at $6De$, the upper half of the contour has become more circular in shape as compared to those of the lower half. It seems that the contour has slowly shifted from a vague square shape to slightly irregular polygon shape. Farther downstream of $20De$ and $30De$, it can be observed in Figs. 19e and 19f that the contours have become more circular in shape, indicating that the flow has reached the self-preservation state. These are basically consistent with the earlier measurements on the mean velocity.

The shapes of the velocity contours at $2De$ and $4De$ may explain why it is difficult to have an accurate measurement of half-width, and thus, the corresponding axis-switching locations are difficult to determine. Besides, the possible dynamics characteristics of the axis switching, that is, it may not happen at fixed locations but may deviate slightly from time to time, as experienced by most of the researchers, may also contribute to the difficulty. The main reason is that the mean velocity profile is not a critical indicator. Thus it should be required to have measurements of the streamwise vorticity and the corresponding contours. These are in progress in our laboratory and will be reported once they are carefully done.

Conclusions

The initial flow condition of the square jet under investigation was found to be laminar. The potential core was detected to end at approximately $5De$. It was found that self-preservation was achieved at $3De$ for mixing layer and $8De$ for both local maximum mean velocity and temperature, as well as the velocity and temperature half-width. The interaction region, if existent, was very short. The Reynolds normal (u' and v') and shear stresses reached self-preservation at $20De$ and $30De$, respectively, whereas the heat flux attained self-preservation at about $35De$. The distribution of the turbulent Prandtl number indicated that it might have incurred some errors in the computation fluid mechanics results if the turbulent Prandtl number was treated as a constant value throughout the entire y locations. Under the present jet initial conditions (Table 2), there was axis switching at $1.75De$, $5De$, and $17.5De$ in the contoured nozzle square jet. The large De/δ_{my}, low initial turbulent intensity but strong growth of the centerline normal shear stress and strong amplification of turbulence along the shear layers at both the side and diagonal of the jet should have overcome the adverse effect of the large δ_{mw}/δ_{my}. However, to provide a better comprehension of axis switching, further measurement of the streamwise vorticity is still required.

Acknowledgment

The financial support of Nanyang Technical University Research Grant RP 40/93 is gratefully acknowledged.

References

[1]Gutmark, E. J., and Grinstein, F. F., "Flow Control with Noncircular Jets," *Annual Review of Fluid Mechanics*, Vol. 31, 1999, pp. 239–272.

[2]Tsuchiya, Y., Horikoshi, C., and Sato, T., "On the Spread of Rectangular Jets," *Experiments in Fluids*, Vol. 4, 1986, pp. 197–204.

[3]Quinn, W. R., and Militzer, J., "Experimental and Numerical Study of a Turbulent Free Square Jet," *Physics of Fluids*, Vol. 31, 1988, pp. 1017–1025.

[4]Gutmark, E. J., Schadow, T. P., Parr, T. P., Hanson-Parr, D. M., and Wilson, K. J., "Noncircular Jets in Combustion Systems," *Experiments in Fluids*, Vol. 7, 1989, pp. 248–258.

[5]Quinn, W. R., "Streamwise Evolution of a Square Jet Cross Section," *AIAA Journal*, Vol. 30, 1992, pp. 2852–2857.

[6]Grinstein, F. F., Gutmark, E. J., and Parr, T., "Near Field Dynamics of Subsonic Free Square Jets. A Computational and Experimental Study," *Physics of Fluids*, Vol. 7, 1995, pp. 1483–1497.

[7]Zaman, K. B. M. Q., "Axis Switching and Spreading of an Asymmetric Jet: The Role of Coherent Structure Dynamics," *Journal of Fluid Mechanics*, Vol. 316, 1996, pp. 1–27.

[8]Tsien, H. S., "On the Design of the Contraction Cone for a Wind Tunnel," *Journal of the Aeronautical Sciences*, Vol. 10, 1943, pp. 68–70.

[9]Chua, L. P., and Goh, E. Y., "Design and Eliminating the Buoyancy Effect of a Heated Circular Jet," *International Communications in Heat and Mass Transfer*, Vol. 21, 1994, pp. 629–639.

[10]Kline, S. J., and McClintock, F. A., "Describing Uncertainties in Single-Sample Experiments," *Mechanical Engineering*, Vol. 75, 1953, pp. 3–9.

[11]Yevdjevich, V. M., "Diffusion of Slot Jets with Finite Length-Width Ratios," Dept. of Earth Resources, Hydraulic Paper 2, Colorado State Univ., Fort Collins, CO, Feb. 1966.

[12]DuPlessis, M. P., Wang, R. L., and Kahawita, R., "Investigation of the Near-Region of a Square Jet," *Journal of Fluids Engineering*, Vol. 96, 1974, pp. 246–251.

[13]Hussain, A. K. M. F., and Clark, A. R., "Upstream Influence on the Near Field of a Plane Turbulent Jet," *Physics of Fluids*, Vol. 20, 1977, pp. 1416–1426.

[14]Chua, L. P., and Antonia, R. A., "Flow Reversal and Intermittency of a Turbulent Jet," *AIAA Journal*, Vol. 27, 1989, pp. 1494–1499.

[15]Browne, L. W. B., Antonia, R. A., and Chua, L. P., "Velocity Vector Cone Angle in Turbulent Flows," *Experiments in Fluids*, Vol. 8, 1989, pp. 13–16.

[16]Chua, L. P., and Antonia, R. A., "Turbulent Prandtl Number in a Circular Jet," *International Journal of Heat and Mass Transfer*, Vol. 33, 1990, pp. 331–339.

[17]Koshigoe, S., Gutmark, E. J., and Schadow, K. C., "Initial Development of Noncircular Jets Leading to Axis Switching," *AIAA Journal*, Vol. 27, 1989, pp. 411–419.

I. Gokalp
Associate Editor